Available online at www.sciencedirect.com
ScienceDirect
Journal of Solid State Chemistry 180 (2007) 1130–1140
JOURNAL OF SOLID STATE CHEMISTRY
www.elsevier.com/locate/jssc

Characterization and acidic properties of Al-SBA-15 materials prepared by post-synthesis alumination of a low-cost ordered mesoporous silica

M. Gómez-Cazalilla[a], J.M. Mérida-Robles[a], A. Gurbani[b], E. Rodríguez-Castellón[a], A. Jiménez-López[a,*]

[a]*Departamento de Química Inorgánica, Cristalografía y Mineralogía (Unidad Asociada al ICP-CSIC), Facultad de Ciencias, Universidad de Málaga, Campus de Teatinos, 29071 Málaga, Spain*
[b]*Instituto de Catálisis y Petroleoquímica, CSIC, Cantoblanco, 28049 Madrid, Spain*

Received 6 October 2006; received in revised form 21 December 2006; accepted 26 December 2006
Available online 1 February 2007

Abstract

A series of Al-containing SBA-15 type materials with different Si/Al ratio, were prepared by post-synthesis modification of a pure highly ordered mesoporous silica SBA-15 obtained by using sodium silicate as silica source, and amphiphilic block copolymer as structure-directing agent. A high level of aluminum incorporation was achieved, reaching an Si/Al ratio of up to 5.5, without any significant loss in the textural properties of SBA-15. These materials were fully characterized by powder X-ray diffraction (XRD), X-ray photoelectron spectroscopy (XPS), ^{27}Al NMR spectroscopy, and N_2 adsorption at 77 K. The acid properties of these materials have been evaluated by NH_3-TPD, adsorption of pyridine and deuterated acetonitrile coupled to FTIR spectroscopy. The effective acidity of these materials was evaluated using two catalytic reactions: 2-propanol dehydrogenation and 1-butene isomerization. The adsorption of basic probe molecules and the catalytic behavior revealed an evolution of the acid properties with the Al content. These studies have shown that the Al-SBA-15 materials contain Brønsted and Lewis acid sites with medium acidity which makes them appropriate to be used as acid catalysts in heterogeneous catalysis, catalytic supports, and adsorbents.

Keywords: Mesoporous solids; aluminum oxide; Non-ionic surfactant; Sodium silicate; Acidity

1. Introduction

Ordered mesoporous silica was first reported independently by Mobil scientists [1] and by Kuroda's group [2,3] in the early 1990s. These materials are characterized by a regular array of pores, in the 2.0–10.0 nm range, with uniform diameter, high specific surface area, and pore volume which are advantageous for the adsorption and catalytic conversion of bulky molecules. The number of research papers dealing not only with mesoporous silica, but also with other oxides, such as alumina, titania, and zirconia, has grown tremendously during the last decade [4]. The vast majority of these papers deal with syntheses from organosilicates as silica source, which are quite expensive. As a result, economic considerations have recently triggered an interest in the use of an inexpensive inorganic silicate as starting material, in order to increase the number of viable applications for the material.

On another front, a great variety of cationic, anionic, and neutral surfactant molecules have been used in the synthesis of ordered mesoporous silica- or non-silica [5,6]. Non-ionic surfactants give important commercial advantages in comparison to ionic surfactants. They are easily removable, non-toxic, biodegradable and relatively cheap. Pinnavaia et al. [7] have reported on the synthesis of MSU-X mesoporus materials with several non-ionic surfactants. Stucky et al. [8] have studied the synthesis of a highly ordered hexagonal mesoporous silica SBA-15 with ultra-large $d(100)$ spacings of 10.4–32.0 nm by using poly(alkylene oxide) triblock copolymer. SBA-15 has BET surface areas of 690–1040 $m^2 g^{-1}$, large pore sizes of 4.6–30.0 nm, and unusually large pore volumes of up to 2.5 $cm^3 g^{-1}$, with silica wall thicknesses ranging from 3.1 to 6.4 nm. The

*Corresponding author. Fax: +34 952137534.
E-mail address: ajimenezl@uma.es (A. Jiménez-López).

0022-4596/$ - see front matter © 2007 Elsevier Inc. All rights reserved.
doi:10.1016/j.jssc.2006.12.038

improved hydrothermal and thermal stability make them some of the most promising catalytic materials. However, the synthetic procedures are not as commercially viable due to the use of tetraethyl orthosilicate as a silica source. Roziere et al. [9] prepared mesoporous monolithic silicas and aluminosilicates using commercial non-ionic surfactants as structure-directing agents; and large mesoporosus organosilicas using triblock copolymers as structure-directing species [10]. Guth et al. [11] have, recently, reported the synthesis of mesoporous silica material based on the use of non-ionic surfactant and sodium silicate, but the materials obtained exhibit irregular or disordered channel connectivity and broad pore size distributions. More recently, Kim and Stucky [12] have developed a new synthetic method for highly ordered mesoporous silica using sodium metasilicate as a silica source and amphiphilic block copolymers as the structure-directing agents.

Moreover, the substituents such as aluminum, titanium and zirconium can be incorporated into the silica framework to obtain materials for applications such as catalysis and ion exchange. For this reason, we recently prepared a series of zirconium-doped silica with different Si/Zr molar ratios using a sol–gel methodology, starting from inorganic Zr and Si precursors, different to alkoxides, and using polyethyleneoxide as a non-ionic surfactant template structure-directing agent [13]. These materials are excellent candidates to be used in heterogeneous catalysis as both acid catalysts and supports [14,15]. Among the metal-substituted mesoporous materials, aluminum-incorporated mesoporous materials have great potential in moderating acid-catalyzed reactions for large molecules [16–18]. However, it is very difficult to introduce the metal ions directly into SBA-15 due to the easy dissociation of metal-O–Si bonds under strong acidic conditions. In fact, to date, only a few studies on the direct synthesis of Al-SBA-15 have been reported [19–24]. Thus, the post-synthesis method for the alumination of the mesoporous silicas, that are obtained under strongly acid conditions, becomes an appealing alternative [25]. Many studies have shown that aluminum can be effectively incorporated into siliceous MCM-41 and MCM-48 materials via various post-synthesis procedures. The authors claimed that the materials produced via the post-synthesis method have superior structural integrity, acidity, and catalytic activity than those of materials having aluminum incorporated during synthesis [26–29]. However, as of present, few post-synthesis alumination methods for SBA-15 have been reported [30–32]. Recently Kao et al. [33] have shown an efficient route for synthesizing SBA-15 with high-framework aluminum contents (a Si/Al ratio close to 5), without any significant loss in textural properties of SBA-15, by the treatment of pure silica SBA-15 with an aqueous solution of $(NH_4)_3AlF_6$ at room temperature. Zeng et al. [34] have also recently shown that the pH and aluminum concentration in the aqueous solution are important parameters in the preparation of Al-SBA-15 materials by post-synthesis method because they have a direct effect on the acidity of the resulting material.

Here we present the synthesis, characterization and the evaluation of the acid properties of a series of Al-SBA-15 materials with different aluminum content. The preparation of the mesoporous silica was based on the procedure proposed by Kim and Stucky [12] by using sodium silicate as a cheap inorganic silica source and a triblock copolymer (Pluronic P123) as a non-ionic structure-directing agent, but introducing some modifications. A series of Al-SBA-15 materials, with different Si/Al ratio were obtained by post-synthesis alumination as proposed by Zeng et al. [34]. The materials were fully characterized by different physico-chemical methods showing a high-framework aluminum content (up to a bulk Si/Al ratio of 5.5) and good structural integrity. The concentration of acid centers was found to depend on the amount of aluminum incorporated into the siliceous framework. The acid nature of this family of mesoporous solids has been studied by the adsorption of two-probe basic molecules and by catalytic tests of 2-propanol and 1-butene conversion.

2. Experimental section

2.1. Reactants

The silicon source was a sodium silicate solution ($Na_2Si_3O_7$ with 27% SiO_2 and 14% NaOH from Aldrich). Aluminum was incorporated with aluminum chloride ($AlCl_3 \cdot 6H_2O$) from Aldrich. The non-ionic surfactant was triblock poly(ethylene oxide)-*b*-poly(propylene oxide)-*b*-poly(ethylene oxide) copolymer Pluronic P123 ($M_{av} = 5800$, $EO_{20}PO_{70}EO_{20}$) from Aldrich. Analytical-grade sodium hydroxide from Prolabo and tetramethylammonium hydroxide (TMAOH) 25 wt% solution in water from Aldrich were also used.

2.2. Samples preparation

In a typical synthesis, 5 g of Pluronic were added to 200 mL of 0.4 M H_2SO_4 solution. After stirring for a few hours, a clear solution was obtained. Then, 0.2 g of NaOH and 13.3 mL of sodium silicate solution were added at room temperature with magnetic stirring. The resulting gel mixture was stirred for 5 days at room temperature, the final pH was about 1. The solid product was recovered by filtration, washed several times with water and dried overnight at 333 K. Finally, the material was heated in air at a heating rate of 10 K min^{-1} to 823 K and maintained at this temperature for 6 h.

Alumination of this pure silica Si-SBA-15 material was carried out by mixing different volumes of aqueous solution 1.2 M of $AlCl_3 \cdot 6H_2O$ with 25 mL of TMAOH 5.5 wt% solution in water. The resulting acid solution (pH 3.5–4) was heated to 353 K until a clear solution was obtained (ca. 1 h). Then 1.5 g of the pure silica Si-SBA-15 was added at room temperature and this mixture was

maintained at 353 K for 3 h. After filtration, washing with water and drying at 333 K, the products were calcined with a heating rate of 10 K min^{-1} to 823 K and maintained at this temperature for 6 h. The volume of the $AlCl_3 \cdot 6H_2O$ aqueous solution was varied to achieve Si/Al molar ratios of 25, 10, 5, and 2.5. The ratio [TMAOH]/[Al] = 2.5 was used for all materials. These aluminated samples were labeled as Al-*x*-SBA-15, where *x* represents the Si/Al ratio of the initial mixtures.

The concentration of the $AlCl_3 \cdot 6H_2O$ solution and the ratio [TMAOH]/[Al] in the alumination solution play an important role on the Si/Al ratio in the resulting material. The values selected in this study were based on a previous study [34], in which the authors concluded that the amount of inserted Al is higher when either the concentration of the Al solution or the [TMAOH]/[Al] ratio is increased.

2.3. Materials characterization

The Al contents of the samples were measured by atomic absorption spectroscopy using a Varian SPECTRAA50. Powder X-ray diffraction (XRD) patterns were recorded on a Siemens D5000 diffractometer using Cu$K\alpha$ radiation and a graphite monochromator. Scanning electron micrographs (SEM) were obtained by using a JEOL SM 840. Samples were placed over an aluminum drum and covered with a gold film using a JEOL Ion Sputter JFC 1100. Surface studies by X-ray photoelectron spectroscopy (XPS) were carried out in a Physical Eletronics PHI-750 spectrometer, equipped with X-ray radiation sources of Mg$K\alpha$ (1253.6 eV). In order to measure binding energies ($\pm$0.1 eV), the C 1*s* signal of the adventitious carbon was used as reference at 284.8 eV. All samples were previously degassed for 12 h under ultra-high vacuum ($<1.3 \times 10^{-6}$ Pa) prior to the analysis. The modified Auger parameter of Al (α') was calculated using the following equation [35]:

$$\alpha' = 1253.6 + \mathrm{KE}(\mathrm{Al_{KLL}}) - \mathrm{KE}(\mathrm{Al}\ 2p),$$

where $\mathrm{KE}(\mathrm{Al_{KLL}})$ is the kinetic energy of the Auger electron of $\mathrm{Al_{KLL}}$ and KE(Al 2*p*) the kinetic energy of the photoelectron Al 2*p*.

Nitrogen adsorption–desorption isotherms at 77 K were obtained using an automatic Micromeritics ASAP 2020, previously outgassing the samples at 473 K and 1×10^{-2} Pa overnight. BET specific surface areas were evaluated using 0.162 nm^2 as the cross-sectional area of the adsorbed nitrogen molecule. Pore size distributions were calculated with the Cranston and Inkley method for cylindrical pores [36].

Temperature-programmed desorption of ammonia (NH_3-TPD) was used to determine the total acidity of the samples. Before the adsorption of ammonia at 373 K, the samples were heated to 823 K in a He flow. The ammonia desorbed between 373 and 823 K (heating rate of 10 K min^{-1}) was analyzed by an on-line gas chromatograph (Shimadzu GC-14A) provided with a TC detector.

FTIR spectra of adsorbed pyridine (Py-IR) were recorded on a Shimadzu 8300 spectrometer. Self-supported wafers of the samples with a weight/surface ratio of about 12 mg cm^{-2} were placed in a vacuum cell with greaseless stopcocks and CaF_2 windows. The samples were evacuated at 523 K and 10^{-2} Pa overnight, exposed to pyridine vapors at room temperature for 15 min and then outgassed at different temperatures.

Infrared spectra of the chemisorbed deuterated acetonitrile (CD_3CN) were recorded at room temperature on a Nicolet 5700 Fourier transform spectrophotometer equipped with an Hg–Cd–Te cryodetector, working in the 4000–650 cm^{-1} wavenumber range at a resolution of 4 cm^{-1} and by averaging over 256 scans. The samples were pressed into self-supporting wafers (ca. 12 mg cm^{-2}) and placed in a sample holder, which was loaded in an infrared vacuum cell equipped with greaseless stopcocks and KBr windows. Prior to the adsorption of CD_3CN at room temperature (5 Torr, 1 Torr = 133.33 N m^{-2}) samples were outgassed (residual pressure $<10^{-4}$ mbar). To remove the fraction of physically adsorbed molecules and to study the absorption bands stability, samples were evacuated at different time and temperatures. Net infrared spectra were obtained by subtracting the sample background spectrum and the cell windows from the whole spectrum.

Single-pulse spectra were recorded on a Bruker DRX400 spectrometer with a magnetic field of 9.36 T and equipped with a multinuclear probe. Powdered samples were packed in 4 mm zirconia rotors and spun at 10 kHz. ^{27}Al MAS-NMR spectra were recorded at 104.26 MHz with a $\pi/20$ pulse width of 1.6 μs and delay time of 3 s. The chemical shifts are reported in ppm from *t* 0.1 M solutions of $AlCl_3$.

The catalytic decomposition of 2-propanol was used as a test reaction for the study of the effective acidity. A fixed-bed tubular glass reactor working at atmospheric pressure was used for a solid charge of 30 mg without dilution (0.2–0.3 mm particle size). Samples were pretreated at 473 K in a helium flow for 3 h (60 ml min^{-1}). Isopropanol was fed into the reactor by flowing He (dried through a molecular sieve, flow rate 25 cm^3 min^{-1}) through a saturator condenser at 303 K, which gave a constant isopropanol flow of 7.5 vol%. None of the samples showed diffusion restrictions. The reaction products were analyzed by an on-line gas chromatograph (Shimadzu GC-14A) provided with an FID and a fused silica capillary column SPB1.

The catalytic isomerization of 1-butene was performed in a tubular glass flow microreactor. The samples (133 mg) were pretreated for 2 h in a He flow at 673 K (30 ml min^{-1}), and experiments were carried out at this temperature. Experiments were performed at $\tau = 0.60 g_{cat} \cdot g^{-1}_{1-but} \cdot h$ and the time on stream was 120 min. The reactant 1-butene and the reaction products were analyzed on-line in a gas chromatograph (Shimadzu GC-14B) equipped with a wide-bore $KCl/AlCl_3$ column. For this reaction, the distribution of *n*-butenes was close to the equilibrium point.

3. Results and discussion

3.1. Elemental analysis, XRD, and morphology

The aluminum content of the samples, determined by atomic absorption, is listed in Table 1. The Si/Al ratios obtained were higher than those added in the initial synthesis mixture. The high Al content in the Al-2.5-SBA-15 sample (Si/Al ratio of 5.5) is comparable to that obtained by other post-synthesis methods recently published [23,32], but by using a Si-SBA-15 obtained with TEOS.

The small-angle powder XRD patterns of calcined Si-SBA-15 and Al-*x*-SBA-15 materials are shown in Fig. 1. All the samples exhibit XRD patterns with a very intense diffraction peak at $2\theta = 1.1^\circ$ and three other weak peaks at $2\theta = 1.9^\circ$, 2.2°, and 3.0°, which can be indexed in a system of hexagonal symmetry as (100), (110), (200), and (210) diffraction planes, respectively. These results are consistent with those previously reported for mesoporous silica prepared from sodium silicate solutions and Pluronic P123 [10]. The XRD diffraction peaks can be indexed to a hexagonal lattice with a d_{100} spacing close to 8.0 nm (shown in Table 1), corresponding to a unit cell parameter a_0 of 9.2 nm, based on the formula $a_0 = 2d_{100}$. After alumination, the XRD patterns indicate that all the samples retain the characteristic patterns of the hexagonal mesostructures.

To establish the morphology of the materials, the SEM reveals that the incorporation of aluminum in Si-SBA-15 pores has no evident effect on the macroscopic morphology of the samples (Fig. 2). The SEM images of the samples show aggregates of regular rod-shaped particles.

Textural properties of the solids were obtained from 77 K nitrogen adsorption/desorption isotherm measurements, which allows the specific surface areas, specific pore volumes, and mesopore size distributions to be calculated, as depicted in Table 1. Fig. 3 gives the adsorption/desorption isotherms and the pore size distributions (inset) of the Si-SBA-15 and Al-2.5-SBA-15 materials. All patterns showed N_2 isotherms typical of mesoporous structures (type IV). The presence of pore filling steps within a narrow range of p/p_0 along with the reversibility of the step is consistent with the presence of tubular pores of uniform size [37]. Pore size distributions, obtained by using the Cranston and Inkley method for cylindrical pores, are narrow with the maximum pore diameters at 4.25 nm for the entire series of materials. The BET specific surface areas and the accumulated pore volumes consistently decreased with the amount of incorporated aluminum, with the maximum reduction in the BET surface area being 37.8% for the sample with the highest aluminum content. Table 1 also indicates that the pore volume decreases in the same direction. This could be an indication of the aluminum incorporation to pore surface by modifying its pore diameter, probably taking place by a partial substitution of Si atoms when the Al content is low and by the formation of Al_xO_y, on the external surface of the

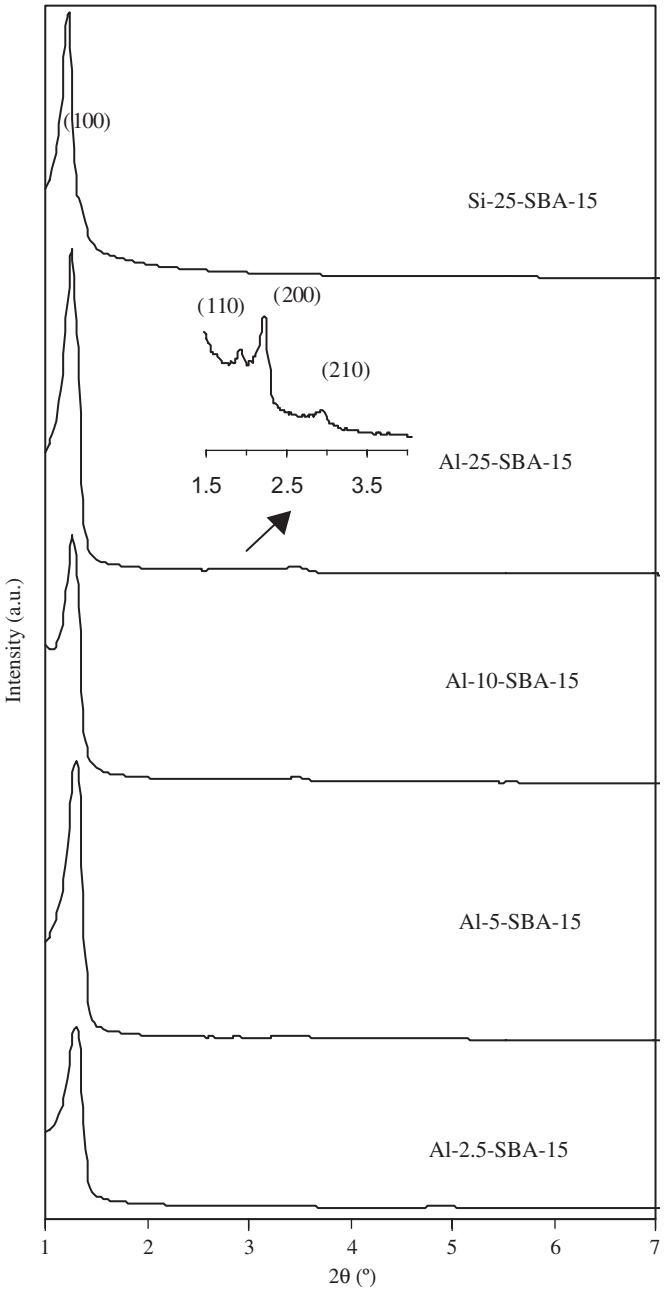

Fig. 1. Powder X-ray diffraction patterns of calcined Al-*x*-SBA-15 and Si-SBA-15 materials.

Table 1
Elemental composition and textural properties of the materials

Sample	Si/Al	d_{100} (nm)	S_{BET} ($m^2\,g^{-1}$)	V_p[a] ($cm^3\,g^{-1}$)
Si-SBA-15	∞	7.61	548.8	0.40
Al-25-SBA-15	49.0	7.83	435.5	0.37
Al-10-SBA-15	21.1	7.83	401.8	0.34
Al-5-SBA-15	14.0	7.72	396.7	0.33
Al-2.5-SBA-15	5.5	7.72	341.1	0.29

[a] V_p at $P/P_0 = 0.95$.

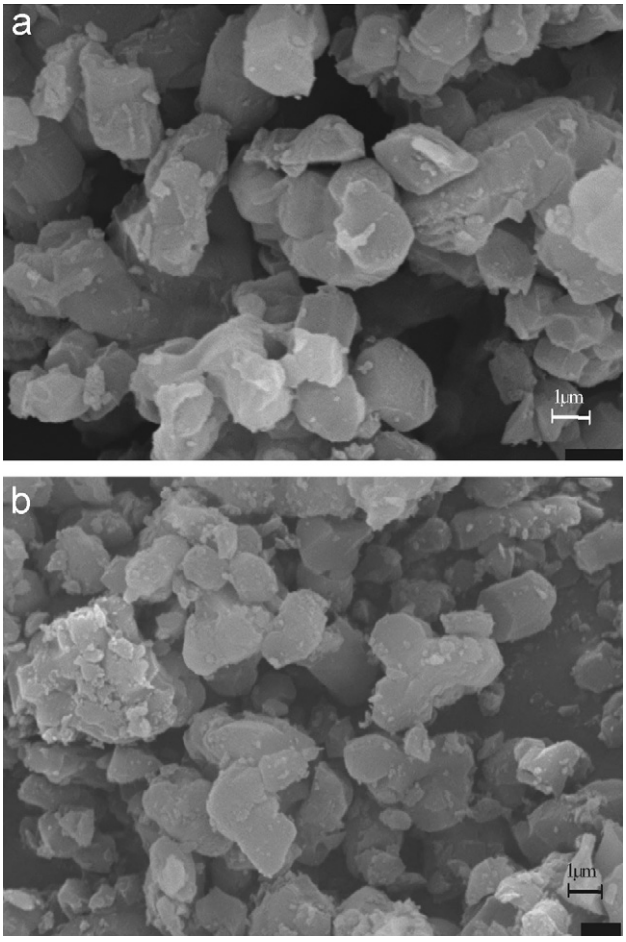

Fig. 2. SEM micrographs of: (a) Si-SBA-15 and (b) Al-2.5-SBA-15 materials.

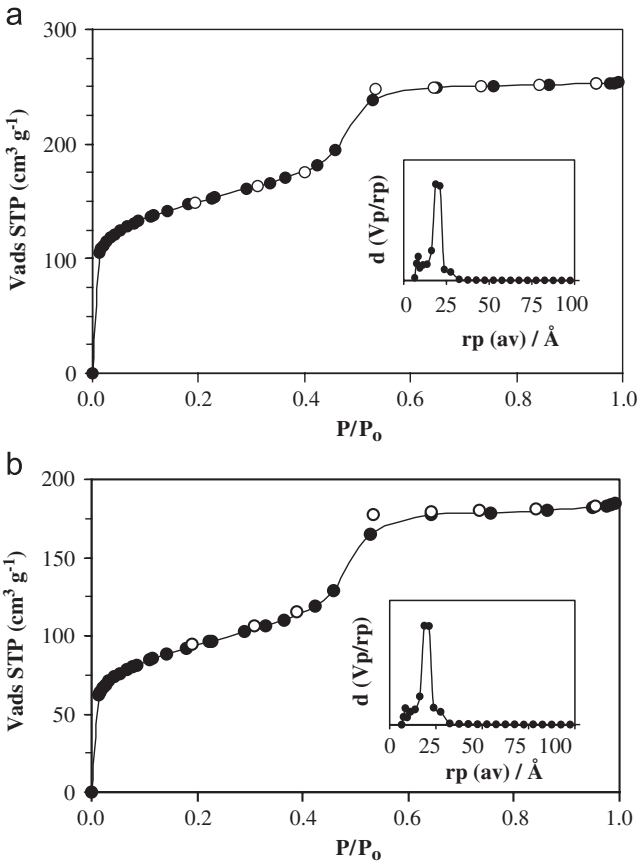

Fig. 3. N_2 adsorption–desorption isotherms at 77 K and the corresponding pore size distributions for: (a) Si-SBA-15 and (b) Al-2.5-SBA-15 materials.

mesoporous silica, for the samples with the highest Al content. These results will be confirmed later by XPS and ^{27}Al NMR studies.

3.2. X-ray photoelectron spectroscopic characterization

In order to get insights into the surface composition, XPS was also employed in this study. Table 2 shows the BE values obtained for Al 2*p*, Si 2*p*, and O 1*s*, and the Si/Al atomic ratios determined by XPS for the series of calcined materials. The surface Si/Al atomic ratios are, for all the materials, lower than those used in the synthesis and those obtained by chemical analysis. This result is to be expected since aluminum has been incorporated by post-synthesis and consequently, aluminum atoms will be preferentially located on the inner surface of pores. The BE of the Al 2*p* peak appears at 74.4 eV for all materials. According to Pashutski et al. [38], three binding energies of Al 2*p* with values of 73.0, 74.5, and 75.4 eV, were found in the study of O_2 adsorption on Al(100), which were assigned to pure Al, Al_xOy ($x/y = 3{:}1$ or 1:1) and Al_2O_3, respectively. Accordingly, the value of 74.4 eV for BE indicates that the Al phase of the Al-*x*-SBA-15 materials can be assigned to Al_xOy ($x/y = 3{:}1$ or 1:1), where Al is less oxidized than Al_2O_3. The Al moieties anchored inside the pores of Si-SBA-15 by the reaction with silanol groups were oxidized through the calcination step. The presence of Al_xO_y with aluminum in low oxygen coordination can confer acidic properties on these solids. On the other hand, the Si *2p* and O 1*s* signals are symmetrical and centered at ca. 103 and 532.3 eV, respectively, which correspond to signals of these elements in these types of compounds.

It is well documented that Al 2p binding energy does not give information to distinguish tetrahedral from octahedral Al [35,39], but it is possible to get more information for identifying the chemical environment of Al by studying the Auger parameter (α'). This parameter is independent of the sample charging. In aluminosilicates, Al α' values depend on the polarizability of the near-neighboring oxygen atoms, i.e., on the coordination. Thus, α' values higher than 1461.0 eV are characteristic of octahedral Al, whereas tetrahedral Al exhibits α' values lower than 1460.4 eV.

Fig. 4 shows the Al KLL spectra for the Al-containing samples. Al-25-SBA-15 shows a unique signal at 1385.2 eV, whereas the other samples exhibit two peaks of different intensities at −1384.4 and −1387.9 eV, respectively. The

Table 2
Binding energy (eV), surface Si/Al atomic ratio, and modified Auger parameter of aluminum in the series of calcined materials

Sample	Binding energy (eV)					
	Al 2*p*	Si 2*p*	O 1*s*	Si/Al	α' tetrahedral Al(III) (eV)	α' octahedral Al(III) (eV)
Si-SBA-15	—	103.1	532.4	—	—	—
Al-25-SBA-15	74.4	103.2	532.4	18.9	1459.6	—
Al-10-SBA-15	74.4	102.6	532.0	6.4	1458.1	1460.8
Al-5-SBA-15	74.4	102.6	532.0	3.9	1458.8	1461.1
Al-2.5-SBA-15	74.4	102.8	532.1	0.8	1458.8	1461.3

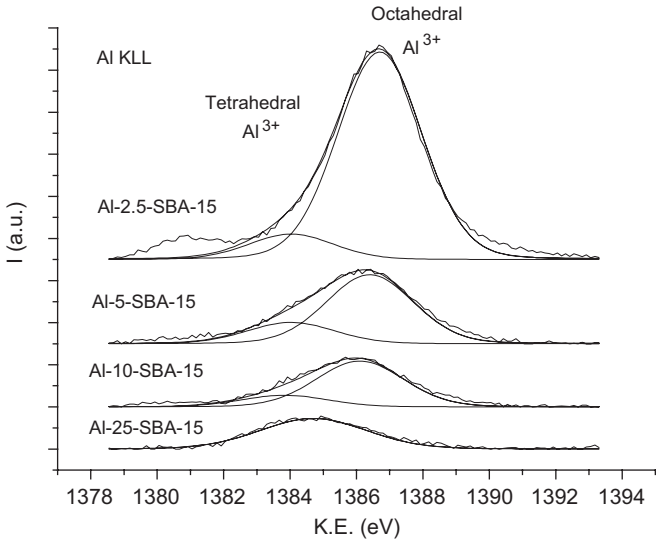

Fig. 4. Al KLL spectra of Al-SBA-15 materials with different Si/Al ratios.

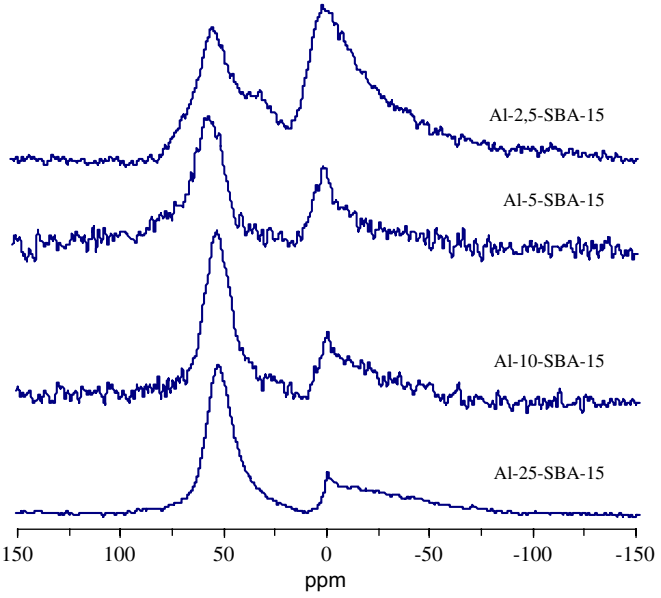

Fig. 5. ^{27}Al MAS NMR spectra of Al-SBA-15 materials with different Si/Al ratios.

second peak becomes more intense when the aluminum loading increases. By using the KE of both peaks the α' parameters have been calculated. These values are compiled in Table 2. α' for Al-25-SBA-15 has a single value of 1459.6, which is characteristic of framework tetrahedral aluminum. All the other samples have two α' values, one on the 1458.1–1458.8 interval, also typical of tetrahedral aluminum and other one at 1460.8–141.3, very similar to that found in the case of γ-Al_2O_3, which are typical of octahedral aluminum. Thus, the sample with the lowest Al content shows a signal assigned to Al in a tetrahedral environment (AlO_4 structural unit), in which Al is covalently bound to four Si atoms via oxygen bridges. The samples with higher Al content also show the signal associated with octahedral Al (AlO_6 structural unit) that increases in intensity with the Al content.

These results reveal the efficiency of this method of incorporation of Al to the SBA-15, because for low Al content it is incorporated to the silica structure by substitution of Si atoms in tetrahedral positions. When the Al content increases, it is deposited in the inner surface of the pores on the primary AlO_4 units leading to the formation of Al_xO_y, where the environment of the Al is octahedral.

3.3. ^{27}Al MAS NMR spectroscopy

The coordination environment of Al atoms in the calcined materials was characterized by ^{27}Al MAS-NMR. The spectra of calcined Al-SBA-15 materials exhibit two resonances (Fig. 5). When the Al content is low the resonance is at 54 ppm, which can be assigned to tetrahedral framework aluminum formed in the mesoporous walls of the material, which is more intense than the other resonance at 0 ppm due to six-coordinate aluminum. In addition, the presence of distorted tetrahedral or five-coordinated aluminum cannot be discarded due to the signal of low intensity observed around 30 ppm [40,41], which is more clearly distinguished in the spectrum of the sample with the highest aluminum content. These results complete the data obtained by XPS analysis, suggesting that aluminum atoms have been successfully incorporated to the pore surface of mesoporous SBA-15 structure by this post-alumination procedure. When aluminum amount is low, loading exhibits preferential tetrahedral coordination, but when the amount of aluminum increases the formation of Al_xO_y takes place.

3.4. Total surface acidity measurement by temperature-programmed desorption of ammonia (NH_3-TPD)

The acidity of the Al-*x*-SBA-15 materials was studied by different methods. One was the temperature-programmed desorption of ammonia (NH_3-TPD) which provides information on the total acidity of the solids, since ammonia is a suitable probe molecule due to its small size and high basicity, which allows it to interact with the majority of acid sites. Thus, the amount of ammonia desorbed at some characteristic temperatures is taken as a measurement of the number of acid centers, while the temperature range in which the ammonia is desorbed is an indicator of the strength of the acid sites. The integration of the curves representing the amount of NH_3 desorbed as a function of the temperature, using different temperature ranges, provides us with the histograms displayed in Fig. 6. The total acidity increases with the aluminum content, to arrive at a value of 817 μmol $NH_3\,g^{-1}$ for the Al-2.5-SBA-15 material. Moreover, the total acidity is very similar for the two materials with the highest Al content. This result can be explained taking into account that only the external and deficiently coordinated aluminum atoms are able to neutralize ammonia molecules. The ammonia desorption reaches its maximum between 373 and 573 K, which is indicative of the mild acidity of these materials. These results indicate that the incorporation of aluminum into the Si-SBA-15 material by post-synthesis is a useful tool to adjust the acidic properties of mesoporous molecular sieves to achieve materials with mild acidity properties.

3.5. Characterization by IR spectroscopy

3.5.1. Skeletal FTIR studies

The IR lattice vibration spectra in the 400–2000 cm^{-1} of calcined samples show the bands resulting from a typical siliceous material, with a main band at 1080 cm^{-1} together with a shoulder at 1227 cm^{-1}, due to asymmetric Si–O–Si stretching modes. There is also a weaker band at 800 cm^{-1}, due to Si–O–Si symmetric stretching modes and a strong band at 458 cm^{-1}, due to rocking Si–O–Si (Fig. 7). It is noteworthy that the incorporation of aluminum causes a decrease in intensity of the component assigned to the Si-(OH) stretching mode at 950 cm^{-1}. This result is understandable with the post-synthesis incorporation of aluminum, since it is introduced into the mesoporous walls via a condensation process of the oxo-hydroxo species of aluminum with the silicon species, such as the Si-(OH) terminal groups.

3.5.2. Surface acidity characterization by adsorption of probe basic molecules coupled to FTIR spectroscopy

To complete the study of the surface acidity and to evaluate the strength and types of acid sites of this family of materials, the absorption of pyridine and deuterated acetonitrile (CD_3CN) coupled to IR spectroscopy was carried out.

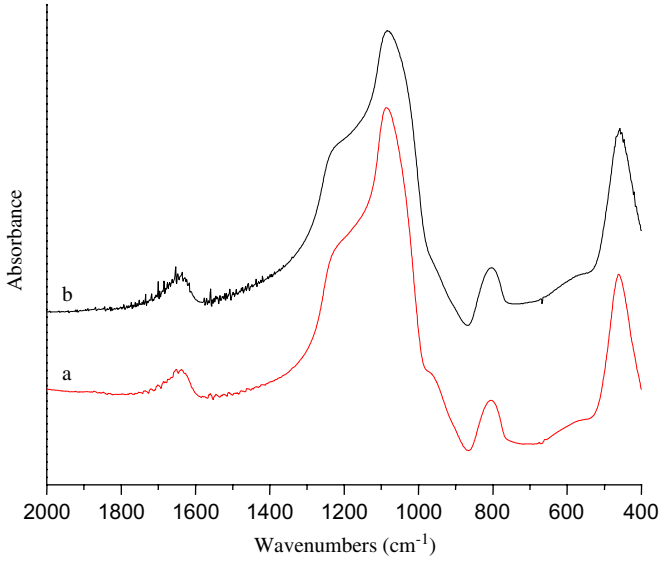

Fig. 7. FTIR skeletal spectra of: (a) Si-SBA-15 and (b) Al-2.5-SBA-15 in KBr.

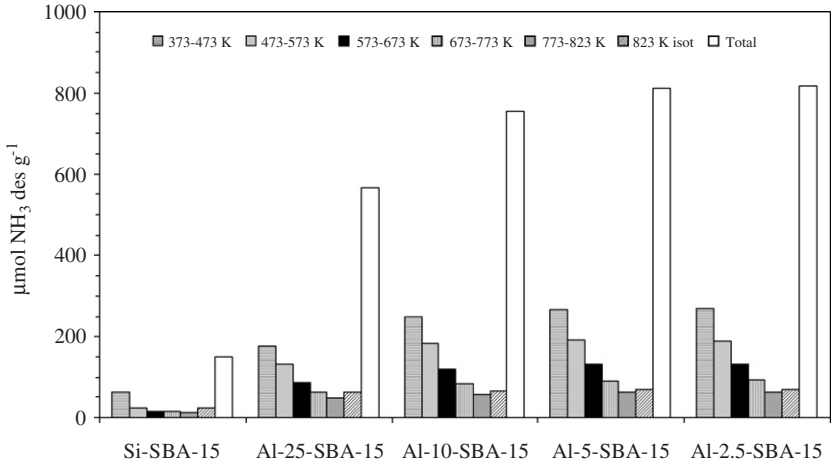

Fig. 6. Histogram of NH_3 desorbed as a function of temperature for Si-SBA-15 and Al-*x*-SBA-15 materials.

Pyridine is a weaker basic molecule than ammonia, hence it can only titrate stronger acid sites. However, it is able to neutralize both Brønsted and Lewis acid sites. The bands at 1545 and 1638 cm^{-1}, and at 1454 and 1620 cm^{-1} are assigned to pyridine adsorbed on the Brønsted and Lewis acid sites, respectively. However, the band at 1490 cm^{-1} is associated with both Lewis and Brønsted acid sites [42,43]. Fig. 8 shows the FTIR spectra of pyridine adsorbed on Si-SBA-15 and Al-2.5-SBA-15 materials, recorded in the range of 1700–1400 cm^{-1}, and outgassed at different temperatures, to estimate the strength of the acidity. The IR spectra reveal the existence of Lewis acid sites on mesoporous silica, shown by the band observed at 1454 cm^{-1}, after outgassing at room temperature. This band disappears after outgassing at a very low temperature (373 K). A higher temperature, above 473 K, is needed to completely remove the pyridine adsorbed on Lewis acid sites for the samples containing aluminum. The IR spectra of the aluminated samples also shows a weak peak at 1545 cm^{-1} associated with the pyridine adsorbed on the Brønsted acid sites, which is even observed at 573 K. The presence of pyridine molecules adsorbed at this temperature indicates the presence of acid sites at least with moderate strength. We can assume that the incorporation of Al gives rise to a small amount of moderate–strong Brønsted acid sites in the form of Si–O(H)–Al bridges. The low temperature at which pyridine is desorbed clearly indicates that the acid sites of the Al-*x*-SBA-15 materials are not strong, as shown before by NH_3-TDP.

The acetonitrile is also used as a probe molecule to elucidate the acid strength of solids since the CN-stretching mode shifts upward by interaction with the electron-withdrawing Lewis and Brønsted acid sites [44,45]. Deuterated acetonitrile was used in order to avoid masking of this vibration band by the Fermi resonance resulting from the ν_{CN} band and the $\delta_{s(CH_3)} + \nu_{C-C}$ combination band. Valuable information about the strength of the Lewis acid sites can be obtained from the position of coordinated CD_3CN in the region 2300–2350 cm^{-1}, since the ν_{CN} band moves towards higher frequencies with the strength of Lewis acid sites.

Fig. 9 shows the infrared spectra after the adsorption of CD_3CN on the studied materials at room temperature and

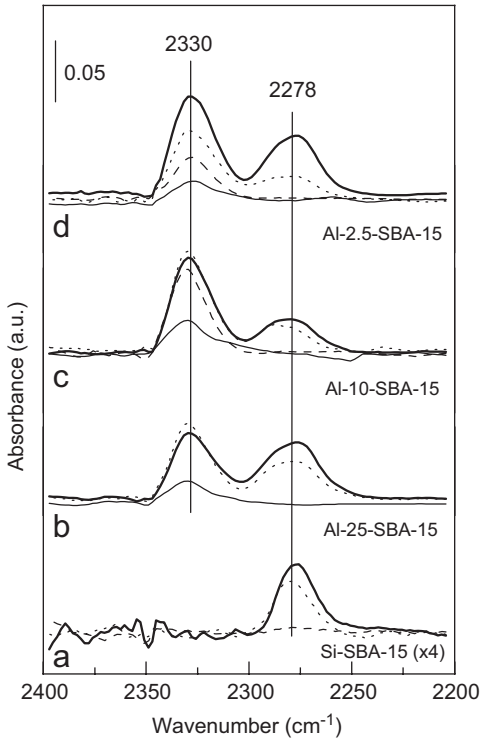

Fig. 9. IR spectra of adsorbed CD_3CN of: (a) Si-SBA-15, (b) Al-25-SBA-15, (c) Al-10-SBA-15, and (d) Al-2.5-SBA-15. Evacuated at room temperature for 10 min (thick solid line), 30 min (dotted line), 10 min at 373 K (dashed line), and 10 min at 473 K (solid line).

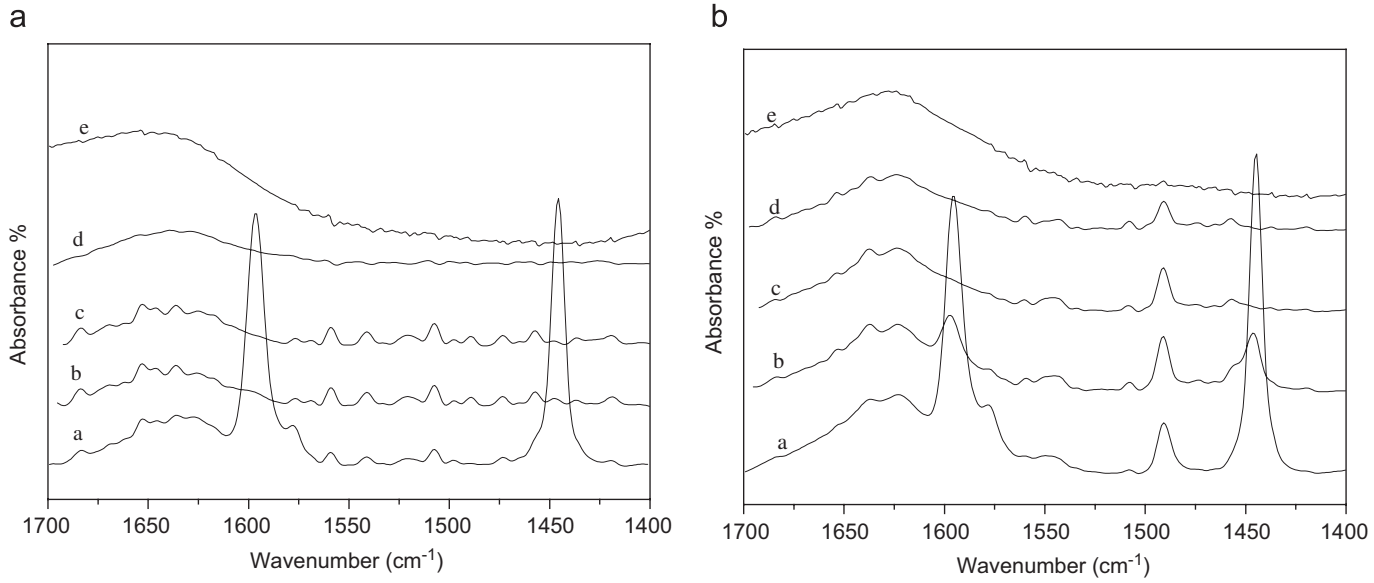

Fig. 8. IR spectra of adsorbed pyridine on: (a) Si-SBA-15 and (b) Al-2.5-SBA-15, after outgassing (a) RT, (b) 373 K, (c) 473 K, (d) 573 K, and (e) reference.

after different periods of evacuation, at 373 and 473 K. Pristine mesoporous silica was also studied as a reference. All materials exhibited an absorption band centered at 2278 cm^{-1}, attributed to CD_3CN molecules weakly interacting with the OH groups [46,47]. This band disappears after treatment at 473 K. The presence of aluminum increases the number of acid Brønsted sites, since the intensity of this band is fourfold to that of the pristine Si-SBA-15. The assignment is confirmed by the parallel increase in the band intensity of the hydroxyl groups during outgassing. The materials containing aluminum show another band centered at 2330 cm^{-1} corresponding to CD_3CN adsorbed on Lewis acid sites with a considerable acid strength. On the other hand, the intensity of this band increases with the Al loading. The degasification at room temperature provokes that the intensity of this band diminishes progressively for the sample with the highest Al content, indicating the presence of acid sites of different strength. However, for samples with lower Al loadings, Al-10-SBA-15 and Al-25-SBA-15, the intensity of this band is only affected when the solid is evacuated at 473 K, revealing the presence of stronger acid sites. Thus the strength of the Lewis acid sites is related to the Al content. The samples with low Al content exhibit by ^{27}Al-NMR the presence of only tetrahedral aluminum for resonances >0 ppm, whereas Al-2.5-SBA-15 material shows both tetrahedral and five-coordinated aluminum, being the last weak acid sites.

3.6. Characterization of the surface acidity by catalytic reactivity

3.6.1. Isopropanol dehydration

Isopropanol conversion and 1-butene isomerization are often applied as catalytic tests to obtain the effective catalytic properties of acid centers. Thus, in the isopropanol conversion, catalysts can be classified according to their degree of acidity in dehydration or the dehydrogenation of propene or acetone, respectively. Thus, dehydration of isopropanol to propylene takes place on acid sites, whereas dehydrogenation to acetone is accomplished on redox or basic sites.

The conversions obtained at different temperatures are compiled in Fig. 10. Whilst Si-SBA-15 is not active in this reaction (at 473 K, 2.1% conversion), the solids containing aluminum exhibit very high conversion at this temperature ($\approx$100% conversion). When the reaction is carried out at a lower temperature (448 K), different conversions appear for these solids as a function of the aluminum content. The conversion is higher for the Al-25-SBA-15 material at any reaction temperature. For higher Al contents a decrease in the conversion takes place, indicating that the dispersion of this species on the inner wall of the pores decreases and thus the number of aluminum ions with deficient coordination acting as acid sites becomes reduced. This fact is in good agreement with the results obtained from XPS and ^{27}Al NMR. The selectivity was close to 100% for propene

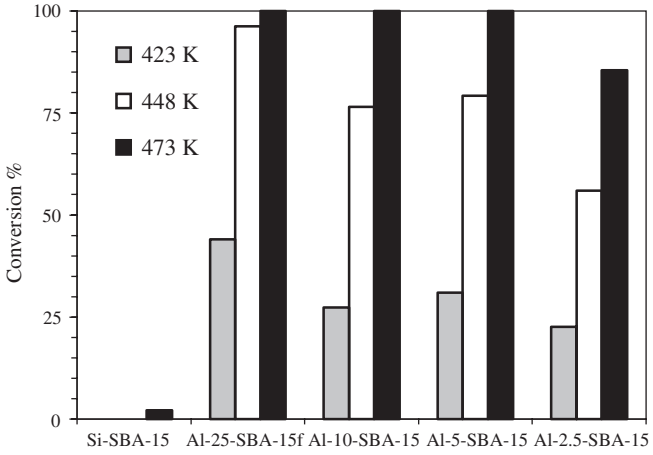

Fig. 10. Variation of the conversion of 2-propanol as a function of the reaction temperature, in the steady state, for Si-SBA-15 and Al-*x*-SBA materials.

for all the Al-*x*-SBA-15 materials at any reaction temperature.

3.6.2. 1-butene isomerization

The isomerization of 1-butene was also selected as a catalytic test to evaluate the acidity of this series of mesoporous materials [48,49]. The reaction is catalyzed by acid centers and occurs through a first step consisting of a double bond shifting, giving 2-butene (*cis* and *trans*), easily reaching the thermodynamic equilibrium. The isomerization to isobutenes in the second reaction step, requires stronger acid sites. Moreover, more acidic catalysts also promote dimerization to octenes, cracking reactions with the formation of C_2, C_3, C_5, and C_6 olefins, and the formation of coke. The type of acidity (Lewis and Brönsted) and the related strength strongly affect the selectivity. Therefore, there are two types of isomerization: a double bond or a methyl migration. Double bond isomerization does not need very strong acidity, and the *cis*/*trans*-2-butenes ratio provides insights into the acid (*cis*/*trans* <1) or basic (*cis*/*trans* >1) nature of the catalyst, while the methyl shift only takes place on strong acid sites. Thus, the formation of isobutene (skeletal isomerization) needs stronger Brönsted acid sites ($H_R < -6.63$) than those required for isomerization or double bond migration ($0.82 > H_R > -4.04$). The reaction occurs on Brönsted acid sites via carbenium ion intermediates in a three-step mechanism. Isomerization of 1-butene is considered to be catalyzed mainly by Brönsted acid sites. If we assume that the double bond isomerization only occurs in all acids, and methyl migration occurs on those acid centers which exhibit an acidity above some given threshold, the selectivity ratio for isobutene/(*cis* + *trans*)-2-butenes will be an approximate measure of the distribution of strong acid site density on the total acid site density. The experimental values, obtained after 3 h on stream at 673 K, are compiled in Table 3.

Table 3
1-butene isomerization data at 673 K

Sample	Conversion (%)	Selectivity (%)				
		cis-2-C_4H_8	*trans*-2-C_4H_8	Iso-C_4H_8	Cracking	$i/(c+t)$
Si-SBA-15	1.1	52.9	47.1	0.0	0.0	0.0
Al-25-SBA-15	80.4	26.5	36.4	26.7	10.4	0.4
Al-10-SBA-15	81.4	25.1	34.4	28.4	12.1	0.5
Al-5-SBA-15	81.8	24.2	33.0	29.7	13.1	0.5
Al-2.5-SBA-15	81.1	24.9	33.8	28.8	12.5	0.5

The Si-SBA-15 material, as expected from the data gathered from NH_3-TPD, is not active in this reaction, while the incorporation of Al into the silica creates acid sites which are able to catalyze the conversion of 1-butene. All the Al-*x*-SBA-15 materials show very similar conversion and selectivity values, probably only due to the Al atoms located on the external surface of the Al_xO_y, which are accessible to the probe molecule. The isobutene/(*cis*+*trans*)-2-butenes ratio was between 0.4 and 0.5 for all the catalysts, indicating that the strength of acid sites is similar and, as shown by NH_3-TPD and pyridine IR, all materials show mild acid sites. This is in good agreement with the low percentage of cracking compounds found. Unfortunately, no relevant information can be obtained from the (*cis*/*trans*)-2-butene ratio because under the experimental conditions used in the present study, the higher levels of conversion favor the subsequent isomerization of *cis*-2-butene to the thermodynamically more stable *trans*-2-butene, thus lowering the observed ratio. In all cases, after 3 h on stream, no deactivation of the catalysts was observed.

4. Conclusions

A series of low-cost SBA-15 with a high-framework Al content were prepared by treating a pure silica, obtained from sodium silicate, with $AlCl_3$ and TMAOH aqueous solutions. XPS and ^{27}Al MAS-NMR studies have confirmed that this post-synthesis method is a good route to incorporate aluminum to a mesoporous silica SBA-15. Pyridine adsorption results show that this series of materials has both Lewis and Brönsted acid sites and, as shown by NH_3-TPD results, the acid centers are mainly medium acidic sites. Moreover, the acidity depends on the amount of aluminum incorporated into the siliceous framework, although the samples with the highest Al contents show very similar behavior in the catalytic test of 2-propanol and 1-butene. This fact could be explained by taking into account that only the superficial Al atoms in the Al-*x*-SBA-15 materials with high Al contents are accessible to probe molecules such as NH_3, pyridine, 2-propanol, and 1-butene.

Acknowledgments

We gratefully acknowledge the funding of this work by the Ministry of Science and Technology (Spain) Project MAT03-2986 and Project MAT06-02465.

References

[1] J.S. Beck, J.C. Vartuli, W.J. Roth, M.E. Leonowicz, C.T. Kresge, K.D. Schmitt, C.T.W. Chu, D.H. Olson, E.W. Sheppard, S.B. Mccullen, J.B. Higgins, J.L. Schlenker, J. Am. Chem. Soc. 114 (1992) 10834.
[2] T. Yanagisawa, T. Shimizu, K. Kuroda, C. Kato, Bull. Chem. Soc. Japan 63 (1990) 988.
[3] S. Inagaki, Y. Fukushima, K. Kuroda, J. Chem. Soc., Chem. Commun. (1993) 680.
[4] A. Berggren, A.E.C. Palmqvist, K. Holmberg, Soft Matter 1 (2005) 219.
[5] P. Van Der Voort, M. Mathieu, F. Mess, E.F. Vansant, J. Phys. Chem. B 102 (1998) 8847.
[6] M. Antonietti, Curr. Opin. Colloid Interface Sci. 6 (2001) 244.
[7] S.A. Bagshaw, E. Prouzet, T.J. Pinnavaia, Science 269 (1995) 1242.
[8] D. Zhao, J. Feng, Q. Huo, N. Melosh, G.H. Fredrickson, B.F. Chmelka, G.D. Stucky, Science 279 (1998) 548;
D. Zhao, Q. Hou, J. Feng, B.F. Chmelka, G.D. Stucky, J. Am. Chem. Soc. 120 (1998) 6024.
[9] J. Roziere, M. Brandhorst, R. Dutartre, M. Jacquin, D.J. Jones, P. Vitse, J. Zajac, J. Mater. Chem. 11 (2001) 3264.
[10] H.G. Zhu, D.J. Jones, J. Zajac, J. Roziere, R. Dutartre, Chem. Commun. (2001) 2568.
[11] L. Sierra, B. Lopez, H. Gil, J.-L. Guth, Adv. Mater. 11 (1999) 307; L. Sierra, J.-L. Guth, Micropor. Mesopor. Mater. 27 (1999) 243.
[12] J.M. Kim, G.D. Stucky, Chem. Commun. (2000) 1159.
[13] A. Infantes-Molina, J. Mérida-Robles, P. Maireles-Torres, E. Finocchio, G. Busca, E. Rodríguez-Castellón, J.L.G. Fierro, A. Jiménez-López, Micropor. Mesopor. Mater. 75 (2004) 23–32.
[14] A. Infantes-Molina, J. Mérida-Robles, E. Rodríguez-Castellón, B. Pawelec, J.L.G. Fierro, A. Jiménez-López, Appl. Catal. A: Gen. 286 (2005) 239.
[15] A. Infantes-Molina, J. Mérida-Robles, E. Rodríguez-Castellón, J.L.G. Fierro, A. Jiménez-López, J. Catal. 240 (2006) 258.
[16] E. Armengol, M. Cano, A. Corma, H. García, M. Navarro, J. Chem. Soc., Chem. Commun. (1995) 519.
[17] R. Mokaya, W. Jones, J. Catal. 172 (1997) 211.
[18] T.R. Pauly, Y. Liu, T.J. Pinnavaia, S.J.L. Brillinge, T.P. Rieker, J. Am. Chem. Soc. 121 (1999) 8835.
[19] Y. Yue, A. Cedeon, J.L. Bonardet, N. Melosh, J.-B. D'Espinose, J. Fraissard, Chem. Commun. (1999) 1967.
[20] S. Wu, Y. Han, Y.C. Zou, J.W. Song, L. Zhao, Y. Di, S.Z. Liu, F.S. Xiao, Chem. Mater. 16 (2004) 486.

[21] Y. Li, W. Zhang, L. Zhang, Q. Yang, Z. Wei, Z. Feng, C. Li, J. Phys. Chem. B 108 (2004) 9739.
[22] W. Li, S.J. Huang, S.B. Liu, M.O. Coppens, Langmuir 21 (2005) 2078.
[23] V.M. Vinus, W. Böhlmann, M. Hartmann, J. Phys. Chem. B 108 (2004) 11496.
[24] Y. Li, Q. Yang, J. Yang, C. Li, J. Porous Mater. 13 (2006) 187.
[25] H.M. Kao, C.C. Ting, S.W. Chao, J. Mol. Catal. A: Chem. 235 (2005) 200.
[26] M. Xu, W. Wang, M. Seiler, A. Buchholz, M. Hunger, J. Phys. Chem. B 106 (2002) 3202.
[27] Q. Xia, K. Hidajat, S. Kawi, J. Catal. 205 (2002) 318.
[28] J.M. Campelo, D. Luna, R. Luque, J.M. Marinas, A.A. Romero, J.J. Calvino, M.P. Rodríguez-Luque, J. Catal. 230 (2005) 336.
[29] R. Luque, J.M. Campelo, D. Luna, J.M. Marinas, A.A. Romero, Micropor. Mesopor. Mater. 84 (2005) 11.
[30] M. Cheng, Z. Wang, K. Sakurai, F. Kumata, T. Saito, T. Komatsu, T. Yashima, Chem. Lett. 2 (1999) 131.
[31] Z. Luan, M. Hartmann, D. Zhao, W. Zhou, L. Kevan, Chem. Mater. 11 (1999) 1621.
[32] S. Sumiya, Y. Oumi, T. Uozumi, T. Sano, J. Mater. Chem. 11 (2001) 1111.
[33] H.M. Kao, C.C. Ting, S.W. Chao, J. Mol. Catal. A: Chem. 235 (2005) 200.
[34] S. Zeng, J. Blanchard, M. Breysse, Y. Shi, X. Shu, H. Nie, D. Li, Micropor. Mesopor. Mater. 85 (2005) 297.
[35] M.J. Remy, M.J. Genet, G. Poncelet, P.F. Lardinois, P.P. Nottè, J. Phys. Chem. 96 (1992) 2614.
[36] R.W. Cranston, F.A. Inkley, Adv. Catal. 9 (1957) 143.
[37] A. Galarneau, D. Desplantier, R. Dutarte, F. Di Renzo, Micropor. Mesopor. Mater. 27 (1999) 297.
[38] A. Pashutski, A. Hoffman, M. Folman, Surf. Sci. 208 (1898) L91.
[39] J.M. Mérida-Robles, P. Olivera Pastor, A. Jiménez López, E. Rodríguez Castellón, J. Phys. Chem. 100 (1996) 14726.
[40] R. Anwander, C. Palm, G. Gerstberger, O. Groeger, G. Engelhardt, Chem. Commun. (1998) 1811.
[41] T.H. Chen, B.H. Wouters, P.J. Grobet, Eur. J. Inorg. Chem. 2 (2000) 281.
[42] E.P. Parris, J. Catal. 2 (1963) 371.
[43] C.A. Emeis, J. Catal. 141 (1993) 347.
[44] A.G. Pelmenschikov, R.A. van Santen, J. Janchen, E. Meijer, J. Phys. Chem. 97 (1993) 11071.
[45] J. Chen, J.M. Thomas, G. Sankar, J. Chem. Soc. Faraday Trans. 90 (1994) 3455.
[46] B. Pawelec, S. Damyanova, R. Mariscal, J.L.G. Fierro, I. Sobrados, J. Sanz, L. Petrov, J. Catal. 223 (2004) 86.
[47] S. Damyanova, L. Dimitrov, R. Mariscal, J.L.G. Fierro, L. Petrov, I. Sobrados, Appl. Catal. A 256 (2003) 183.
[48] A. La Ginestra, P. Patrono, M.L. Berardelli, P. Galli, C. Ferragina, M.A. Massudi, J. Catal. 103 (1987) 346.
[49] P. Patrono, A. La Ginestra, G. Ramis, G. Busca, Appl. Catal. A 107 (1994) 249.